Implementation of two dimensional decomposition for JMA non-hydrostatic model

Kohei Aranami* and Junichi Ishida
Numerical Prediction Division, Japan Meteorological Agency
1-3-4 Otemachi, Chiyoda-ku, Tokyo 100-8122, Japan

1 Introduction

These days massively parallel computers are becoming more popular. The JMA non-hydrostatic model (JMANHM) was parallelized for the distributed memory super computer by using MPI libraries in the way that the entire domain is decomposed in a single direction and each subdomain is assigned to an MPI process. However, the parallel efficiency of the model is not very high with a large number of computational nodes due to the load imbalance among the nodes. Therefore we tried to increase computational efficiency by implementing two dimensional decomposition.

2 Domain decomposition and computational efficiency

We are planning to replace the current operational meso-scale model with JMANHM in 2004. The number of grid points of the operational JMANHM will be 361 × 289 × 40. Therefore first the acceleration rate of this number of grid points was investigated. Figure 1 shows the acceleration rate of JMANHM according to the investigation which was carried out on HITACHI SR8000/E1. This figure shows that the parallel computational ratio does not effectively increase with more than 24 nodes of the computer system.

As is mentioned in section 1, the entire domain of JMANHM was divided only for the latitudinal direction (Fig. 2) in its original design for the parallel treatment, and each subdomain includes 'ghost points' for processes referring to status at the adjacent points. Since the number of the grid points in the north-south direction of each subdomain becomes small with increasing number of nodes, the load imbalance of this decomposition scheme tends to be large with more computational nodes. Thus the parallel efficiency decreases with increasing number of the subdomains, namely, the MPI processes. To improve the computational efficiency, we introduced two dimensional decomposition which is illustrated in Fig. 3. Suppose the grid points 361 × 289 × 40 are handled with 40 MPI processes, the excess of the maximum area size to the minimum is as large as 14 percent in the one dimensional case, while it can be reduced to 4 percent with two dimensional optimal decomposition.

The two dimensional decomposition does not always have advantage over the one dimensional decomposition in computational efficiency, because

- the vector length becomes shorter by the division in x-direction, and
- the communication overhead becomes twice to communicate with all four neighboring processes.

The efficiency depends mainly on the architecture of a particular machine, the number of the model grids, and the number of MPI processes used.

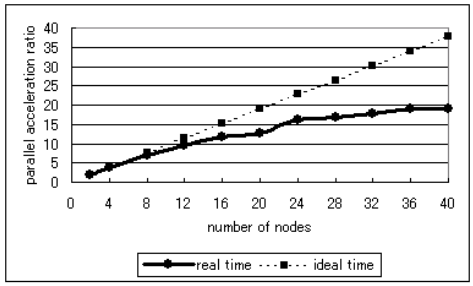

Fig. 1 Acceleration rate.

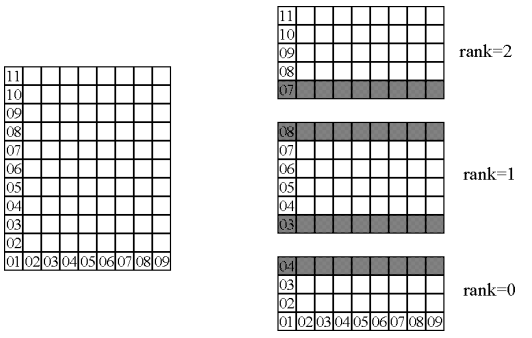

Fig. 2 One dimensional decomposition (case of 3 MPI processes).

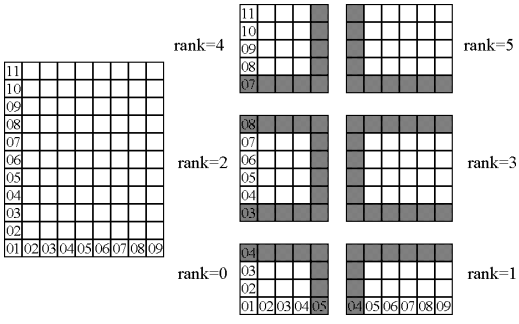

Fig. 3 Two dimensional decomposition (case of 6 MPI processes).

[1]E-mail address of the corresponding author: aranami@naps.kishou.go.jp

3 Validation and comparison of computational cost

Tests for validation and comparison of computational cost were carried out. The tests were conducted with 40 nodes of HITACHI SR8000/E1 which are used for operational NWP by JMA. Each node is assigned one MPI process. 39 nodes are used for computation, and one for data output to execute computation and output simultaneously. Table 1 shows the specifications of the tests. Figures 4 and 5 are the results of six-hour integration of the one dimensional and two dimensional decomposition, respectively. The three-hour accumulated rainfall amount, sea level pressure, and surface wind are shown in these figures. The result of the two dimensional decomposition of 3×13 is almost identical to that of one dimensional decomposition of 1×39 except for trivial differences which reflect the changes of the computational procedure. The computational cost of the two runs are shown in Table 2. The increase of the computational time for-preprocessing becomes less important if forecast time is longer. We got the improvement of 1.7 percent of computational time with the two dimensional decomposition in time integration.

Table 1 Specifications of tests.

number of grid points	$361 \times 289 \times 40$
horizontal resolution	10 km
vertical resolution	40-1180 m
time step	40 sec
initial time	06UTC 20 December 2003
forecast time	6 hours
computer	HITACHI SR8000/E1
number of nodes	40 nodes
peak performance	384 GFLOPS
time integration	split-explicit
advection scheme	horizontally 4th order centered flux form
prognostic variables	$U, V, W, p, \theta, qv, qc, qr, qi, qs, qg$

4 Summary

Two dimensional decomposition is successfully implemented for JMANHM. The procedure improved the computational efficiency even with the current supercomputer at JMA. The new function is expected to have larger impact especially on huge scalar architecture machines where the computational efficiency does not depend on the vector length.

Table 2 Computational elapsed time (sec) of 6 hours forecast.

	1×39	3×13
pre-processing	13.95	20.78
time integration	508.96	500.48
I/O	34.18	32.16
total time	557.09	553.42

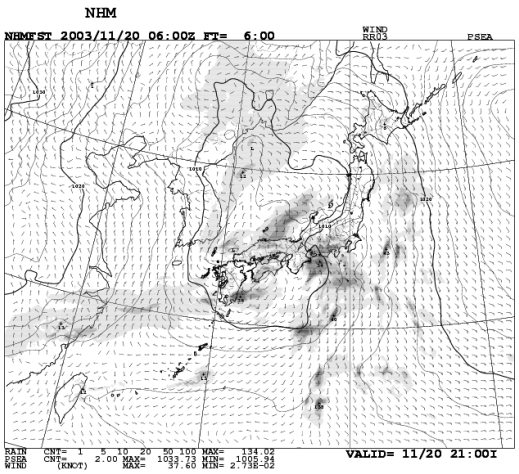

Fig. 4 Result of 1×39.

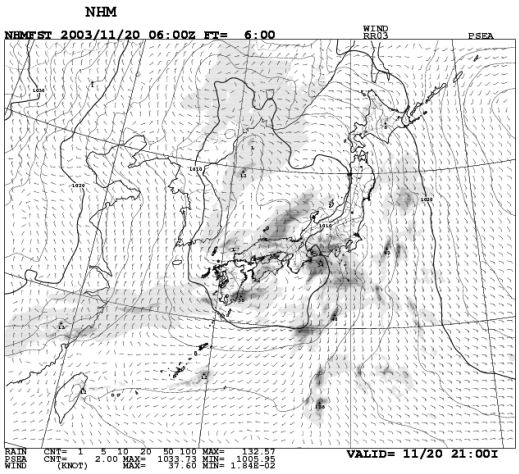

Fig. 5 Result of 3×13.

The ICON dynamical core project: modelling strategies and preliminary results

Luca Bonaventura, Erich Roeckner
Max Planck Institut für Meteorologie
Bundesstraße 55,20146, Hamburg, Germany
e-mail: bonaventura@dkrz.de, roeckner@dkrz.de
Detlev Majewski
Deutscher Wetterdienst
Frankfurter Straße 135, Offenbach, Germany
e-mail: detlev.majewski@dwd.de

The ICON project is a joint development effort of MPIfM and DWD to achieve a unified climate and NWP model. The aim of the project is to overcome many of the shortcomings of current GCMs by appropriate finite volume discretizations on geodesic icosahedral grids.

The model under development in the ICON project will use the fully elastic, nonhydrostatic Navier-Stokes equations, which provide a framework that is sufficiently general for meteorological applications on most scales relevant for numerical weather prediction and climate simulation. In order to couple most consistently stratospheric and mesospheric chemical processes to the dynamics, air will be considered as a multicomponent medium. Conservation of air and tracer mass and consistency of the discretization of the continuity equations for air and tracers will be guaranteed.

As an intermediate step, a semi-implicit discretization for the shallow water equations has been developed. In contrast to other recent discretization approaches on the icosahedral grid (see e.g. [2], [4]) the proposed discretization uses the triangular Delaunay cells of the icosahedral grid as control volumes. It achieves mass and potential enstrophy conservation, thus replicating the results of [3] for standard rectangular C grids. The Raviart-Thomas finite element of order zero is used to reconstruct a uniquely defined velocity field from the velocity components normal to the cell sides, which are the discrete model variables along with the cell averaged value of the geopotential height. A predictor corrector approach along the lines of [1] is used for the discretization of the nonlinear advection terms. The results obtained with a preliminary implementation on an idealized test case (see e.g. [5]) are shown in figure 1. Extensions of the same technique to the Euler equations for global nonhydrostatic modelling are currently being investigated.

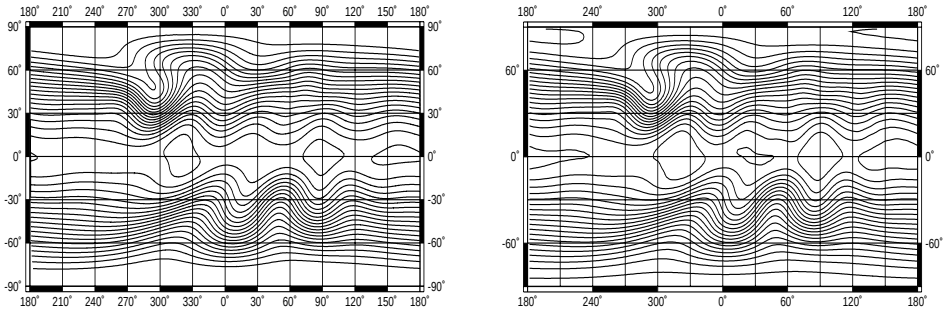

Figure 1: Height field at day 10 for test case 5 of [5] computed by the mass conservative shallow water model on the triangular icosahedral grid with 81920 triangles (left) and by the NCAR reference spectral model at resolution T63 (right). Contours spacing is 50 m.

References

[1] Shian-Jiann Lin and Richard B. Rood. An explicit flux-form semi-Lagrangian shallow water model on the sphere. *Quarterly Journal of the Royal Meteorological Society*, 123:2477–2498, 1997.

[2] Todd D. Ringler, Ross P. Heikes, and David A. Randall. Modeling the atmospheric general circulation using a spherical geodesic grid: A new class of dynamical cores. *Monthly Weather Review*, 128:2471–2490, July 2000.

[3] R. Sadourny. The dynamics of finite difference models of the shallow water equations. *Journal of the Atmospheric Sciences*, 32:680–689, 1975.

[4] H. Tomita, M. Tsugawa, M.Satoh, and K.Goto. Shallow water model on a modified icosahedral grid by using spring dynamics. *Journal of Computational Physics*, 174:579–613, 2001.

[5] David L. Williamson, John B. Drake, James J. Hack, Rüdiger Jakob, and Raul N. Swarztrauber. A standard test set for numerical approximations to the shallow water equations in spherical geometry. *Journal of Computational Physics*, 102:221–224, 1992.

Stablilization of two-time levels semi-implicit algorithms for the Euler system

Pierre Bénard*

* *Centre National de Recherches Météorologiques, Météo-France, Toulouse, France*

1 Introduction

The Euler equations (EE) system is the most natural system for extending the field of NWP to meso-scales. If the numerical solution of the EE system with three time-levels (3-TL) semi-implicit (SI) schemes is straightforward (e.g. Caya and Laprise, 1999), the use of two time-levels (2-TL) SI schemes leads to severe additional difficulties. For those SI schemes in which the linearization reference thermal field is taken as a constant T^*, it can be shown that the solution of the EE system with a 2-TL SI time-scheme is not possible, whatever height or mass types of coordinates are used (Bénard, 2003, B03 hereafter). This difficulty did not manifest itself so drastically for hydrostatic primitive equation (HPE) systems: although the stability domain was reduced when passing from 3-TL to 2-TL discretizations, a practically viable solution was still possible in 2-TL schemes (Simmons and Temperton, 1997).

However, 2-TL schemes are attractive because of their potentially twice effectiveness compared to 3-TL schemes, hence it is worth trying to understand and circumvent this difficulty. Qian et al. (1998) achieved a stabilization of their 2-TL SI EE system by using a large second-order time-decentering ($\epsilon' = 0.5$ in their notations), but this resulted in an loss of accuracy which is not compatible with NWP. An alternative solution is to use an iterative centred implicit (ICI) scheme instead of a SI scheme, as shown in B03 and in the last issue (2003) of this JSC/CAS WGNE series. However, it must be noted that the benefit in efficiency of the 2-TL scheme disappears due to the cost of the iterative algorithm, unless a significant part of the evolution system is left uniterated (e.g. the physical part). This strategy is used in Côté et al (1998).

In this paper, the causes of the difficulty to solve the EE system with 2-TL SI schemes are discussed, and a solution is proposed to circumvent this problem, without loss of accuracy or effectiveness. The material in the present paper is basically drawn and adapted from Bénard (2004, B04 hereafter).

2 Analysis of the problem and proposed solution

As shown in B04 in a classical academic framework allowing stability analyses, the instability of the 2-TL SI EE system originates from the fact that the thermal (explicitely treated) non-linear residuals corresponding to the terms responsible for horizontally propagating gravity and vertically propagating elastic waves systematically have opposite signs. In other words, if T^* is chosen so as to stabilize horizontally propagating gravity waves, then vertically propagating elastic waves will be unstable, and *vice versa*. The problem was of course not present for HPE systems since they did not allow the propagation of elastic waves.

A natural solution to restore systematically the same sign for thermal non-linear thermal residuals in the terms corresponding to the two types of waves, is thus to introduce different values of T^* for each wave sub-system, that is: T^* for the gravity-wave sub-system, and T^*_E for the vertically propagating elastic-wave sub-system. The stability domains for the first and second sub-systems then become $\overline{T} \leq T^*$ and $\overline{T} \geq T^*_E$ respectively in the analytic framework of B04 (which assumes an isothermal $\overline{T}$ atmosphere). As a consequence, choosing $T^*_E < T^*$ allows a non-empty stability domain to be restored. The stability domain for $\overline{T}$ can thus be arbitrarily extended, by setting T^* arbitrarily warm, and T^*_E arbitrarily cold. However, as shown in Simmons and Temperton, 1997, exaggerating this strategy would finally deteriorate the response of the scheme in terms of accuracy. In practice, T^*_E should thus be chosen colder than the coldest likely temperature, and T^* warmer than the warmest likely temperature. Applying this guideline, no significant loss of accuracy is to be expected, compared to a traditional SI scheme. This proposed modification of the SI scheme is straightforward from any pre-existing application.

3 Practical impact

In order to evaluate the potential benefit of the proposed solution for NWP, the modification was tested in real-case conditions with the adiabatic semi-Lagrangian version of the cooperative NWP Aladin-NH limited-area model, used with a 2-TL SI time-discretization. The model was integrated for 3 hours for a randomly-chosen situation consisting of a strong flow over real topography, in a domain which includes the mountainous Pyrénées region. The horizonal resolution is 2.5 km in horizontal directions, and the time-step is 80 s. The vertical coordinate is the classical mass-based hybrid terrain-following coordinate η, and the domain is discretised along 41 irregular layers with a thickness increasing with height, in the usual NWP fashion. Integrations are performed without any time-filter (see B03 for a discussion on the detrimental effects of time-filters in 2-TL SI EE system).

A weak fourth-order horizontal diffusion is applied to avoid the accumulation of energy in the smallest resolved scales during the course of the integration.

Fig. 1 shows the evolution of the whole domain spectral norms (multiplied by 10^4) of the horizontal vorticity ζ and the divergence D for the traditional and modified versions of the 2-TL SI scheme. The traditional SI scheme is used with $T^* = T_E^*$=300K, and the modified SI scheme with T^*=300 K, T_E^*=150 K. The original 2-TL SI scheme is clearly unstable, since the integrations diverge after 11 time-steps, while the modified 2-TL SI scheme behaves stably during the 3 hours of the integration. This experiment clearly indicates a potential advantage of using the modified SI scheme in NWP with 2-TL EE systems. The advantage of the modification is not limited to this case, and was observed in a wide variety of model configurations, including 2D vertical-plane academic flows, and real cases at higher resolution, with and without physics.

4 Conclusion

The EE system can be solved numerically with a 2-TL SI scheme provided that the residual terms corresponding to gravity and vertically propagating elastic waves are enforced to keep the same sign. This can be achieved by defining two SI reference temperatures T^* and T_E^* instead of one in the classical SI scheme. The proposed modification follows from a more general design of SI schemes, in which the linear reference system is no longer obtained through a linearization of the complete system around a given reference state, as explained in B04. If other non-linear residuals impose the use of an iterative scheme, this modification would allow a more diagonal-dominant implicit operator, and thus, a possibly faster convergence.

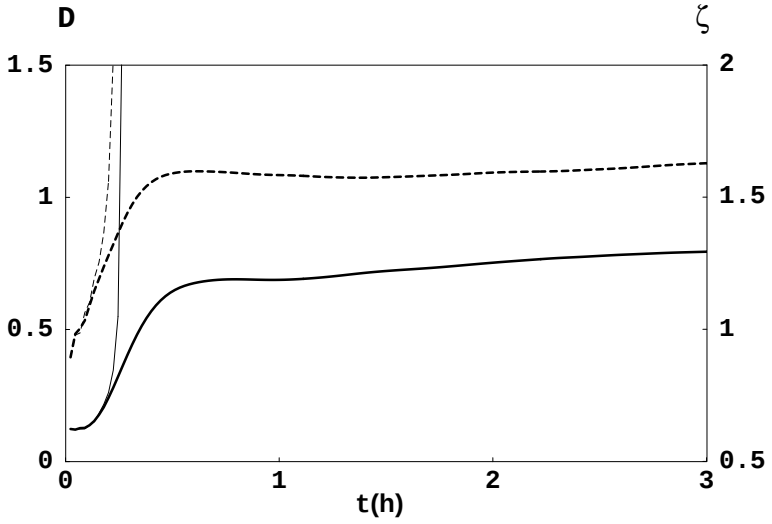

Fig. 1: Evolution of the spectral norm ($\times 10^4$) of vorticity ζ and horizontal divergence D for a real-case with a 2-TL SI EE system. Solid line: vorticity (right axis); dashed line: divergence (left axis); thin line: traditional 2-TL SI scheme; thick line: modified 2-TL SI scheme

References

Bénard, P., 2003: Stability of Semi-Implicit and Iterative Centred-Implicit Time Discretizations for Various Equation Systems Used in NWP. *Mon. Wea. Rev.*, **131**, 2479–2491.

Bénard, P., 2004: On the use of a wider class of linear systems for the design of constant-coefficients semi-implicit time-schemes in NWP. In press at *Mon. Wea. Rev.* (available at the following Internet URL: `http://hal.ccsd.cnrs.fr/view/ccsd-00000881/fr/`)

Caya, D. , and R. Laprise, 1999: A semi-implicit semi-Lagrangian climate model: the Canadian RCM. *Mon. Wea. Rev.*, **127**, 341–362.

Qian, J.-H., F. H. M. Semazzi, and J. S. Scroggs, 1998: A global nonhydrostatic semi-Lagrangian atmospheric model with orography. *Mon. Wea. Rev.*, **126**, 747-771.

Simmons, A. J., and C. Temperton, 1997: Stability of a two-time-level semi-implicit integration scheme for gravity wave motion. *Mon. Wea. Rev.*, **125**, 600-615.

Runge-Kutta Time Integration and High-Order Spatial Discretization – a New Dynamical Core for the LMK

Jochen Förstner, Günther Doms
Deutscher Wetterdienst, Frankfurter Straße 135, 63067 Offenbach am Main
E-mail: jochen.foerstner@dwd.de, guenther.doms@dwd.de

LMK is the name for a new development branch of the *LM* aiming at the meso-gamma scale (horizontal resolution of 2-3 km) and shortest range ("*K*ürzestfrist") forecasts periods (3-18 h). The new dynamical core for the LMK is based on different variants of 2-timelevel Runge-Kutta schemes which are combined with a forward-backward scheme for integrating high-frequency modes of the elastic equations. The first one is the 3rd-order Runge-Kutta scheme used by Wicker and Skamarock (2002) whereas the second one is a total variation diminishing (TVD) variant of 3rd-order (Liu, Osher, and Chan 1994).
For horizontal advection upwind or centered-differences schemes of 3rd- to 6th-order can be used – the operators are formulated in advection form. The vertical advection is normally treated in an implicit way using a Crank-Nicolson scheme and centered-differences in space.
Most slow tendencies such as vertical diffusion, thermal/solar heating, parameterized convection, coriolis force and buoyancy are computed only once using values of the prognostic variables at time step n. These tendencies are fixed during the individual Runge-Kutta steps and contribute to the total slow-mode tendencies which are integrated in several small time steps together with the fast-mode tendencies in a time-splitting sense. In contradiction to this, the whole 3D-advection is computed in each of the Runge-Kutta steps.
In the following the procedure for the TVD-Runge-Kutta scheme is described mathematically in a simplified form – the treatment of the physical forcing terms is omitted and the only operators listed are the ones for advection.

Problem to Solve: $$\frac{\partial \phi}{\partial t} = L^{slow}(\phi) + L^{fast}(\phi)$$

TVD-variant of 3rd-order Runge-Kutta:

$$\phi^{*}_{i,k} = \phi^{n}_{i,k} - \Delta t\, L^{h}_{i}(\phi^{n}) - \Delta t\Big(\beta^{+} L^{v}_{k}(\phi^{*}) + \beta^{-} L^{v}_{k}(\phi^{n})\Big) \qquad = \phi^{0}_{i,k} + \Delta t\, L^{slow}_{i,k}\Big|^{*}_{0}$$

$$\phi^{**}_{i,k} = \frac{3}{4}\phi^{n}_{i,k} + \frac{1}{4}\phi^{*}_{i,k} - \frac{1}{4}\Delta t\, L^{h}_{i}(\phi^{*}) - \frac{1}{4}\Delta t\Big(\beta^{+} L^{v}_{k}(\phi^{**}) + \beta^{-} L^{v}_{k}(\phi^{*})\Big) \qquad = \phi^{0}_{i,k} + \frac{1}{4}\Delta t\, L^{slow}_{i,k}\Big|^{**}_{0}$$

$$\phi^{n+1}_{i,k} = \frac{1}{3}\phi^{n}_{i,k} + \frac{2}{3}\phi^{**}_{i,k} - \frac{2}{3}\Delta t\, L^{h}_{i}(\phi^{**}) - \frac{2}{3}\Delta t\Big(\beta^{+} L^{v}_{k}(\phi^{n+1}) + \beta^{-} L^{v}_{k}(\phi^{**})\Big) \qquad = \phi^{0}_{i,k} + \frac{2}{3}\Delta t\, L^{slow}_{i,k}\Big|^{n+1}_{0}$$

Time-Splitting Method:

1. step:
$$\phi^{0+\Delta\tau}_{i,k} = \phi^{0}_{i,k} + \Delta\tau\, L^{fast}_{i,k}(\phi^{0}) + \Delta\tau\, L^{slow}_{i,k}\Big|^{\times}_{0}$$

remaining steps:
$$\phi^{\tau+\Delta\tau}_{i,k} = \phi^{\tau}_{i,k} + \Delta\tau\, L^{fast}_{i,k}(\phi^{\tau}) + \Delta\tau\, L^{slow}_{i,k}\Big|^{\times}_{0}$$

with $\times = *,\ **$ and $n+1$ in the individual Runge-Kutta steps.

Horizontal and Vertical Operators:

$$L^{h}_{i}(\phi)^{\,(4\text{th})} = \frac{u_i}{12\Delta x}\Big[\phi_{i-2} - 8\big(\phi_{i-1} - \phi_{i+1}\big) - \phi_{i+2}\Big]$$

$$L^{h}_{i}(\phi)^{\,(6\text{th})} = \frac{u_i}{60\Delta x}\Big[-\phi_{i-3} + 9\big(\phi_{i-2} - \phi_{i+2}\big) - 45\big(\phi_{i-1} - \phi_{i+1}\big) + \phi_{i+3}\Big]$$

$$L^{h}_{i}(\phi)^{\,(5\text{th})} = L^{h}_{i}(\phi)^{\,(6\text{th})} + \frac{|u_i|}{60\Delta x}\Big[-\phi_{i-3} + 6\big(\phi_{i-2} + \phi_{i+2}\big) - 15\big(\phi_{i-1} + \phi_{i+1}\big) + 20\phi_i - \phi_{i+3}\Big]$$

$$L^{v}_{k}(\phi)^{\,(2\text{nd})} = \frac{w_k}{2\Delta z}\big(\phi_{k+1} - \phi_{k-1}\big) + M^{v}_{k}(\phi) \qquad \text{with } M^{v}_{k}(\phi)\text{: vertical turbulent mixing term.}$$

Results of an advection test problem of a tracer in a deformational flow field (Durran 1999) are given in Figure 1. The number of time steps used for the stable integration of one deformation cycle is given in the caption for each of the different schemes. The initialized field was a cone with a maximum of 1.0 and a radius of 15 grid spacings.

To test the robustness of the scheme, the winter storm case "Lothar" (26 December 1999) was simulated with the LM. The maximum horizontal velocity during the simulation reaches 108 m/s. For this case the new scheme in the combination TVD-RK-3rd/UP-5th allows a time step of 72 s at a resolution of 7 km compared to a time step of 40 s of the operational Leapfrog/CD-2nd scheme. Results are shown in Figure 2.

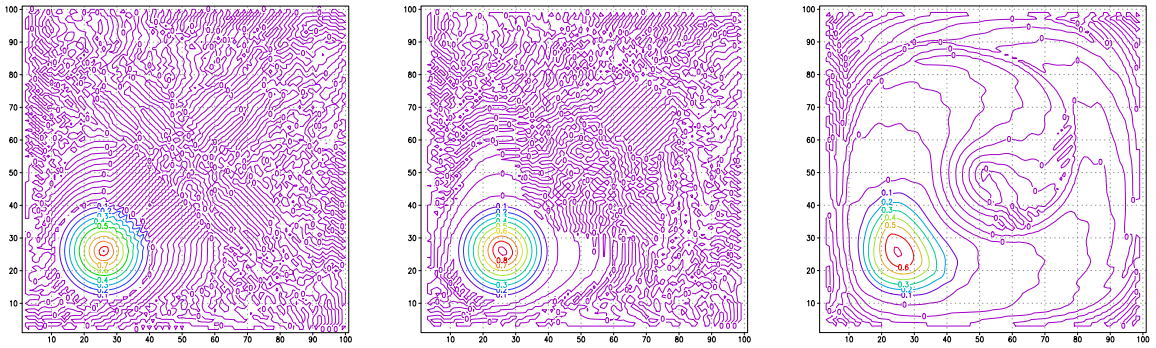

(a) RK-3rd / CD-4th – 670 time steps.

(b) TVD-RK-3rd / CD-4th – 450 time steps.

(c) TVD-RK-3rd / UP-5th – 380 time steps.

Figure 1: *Advection of a tracer in a nondivergent deformational flow (Durran 1999). Simulation results after one deformation cycle.*

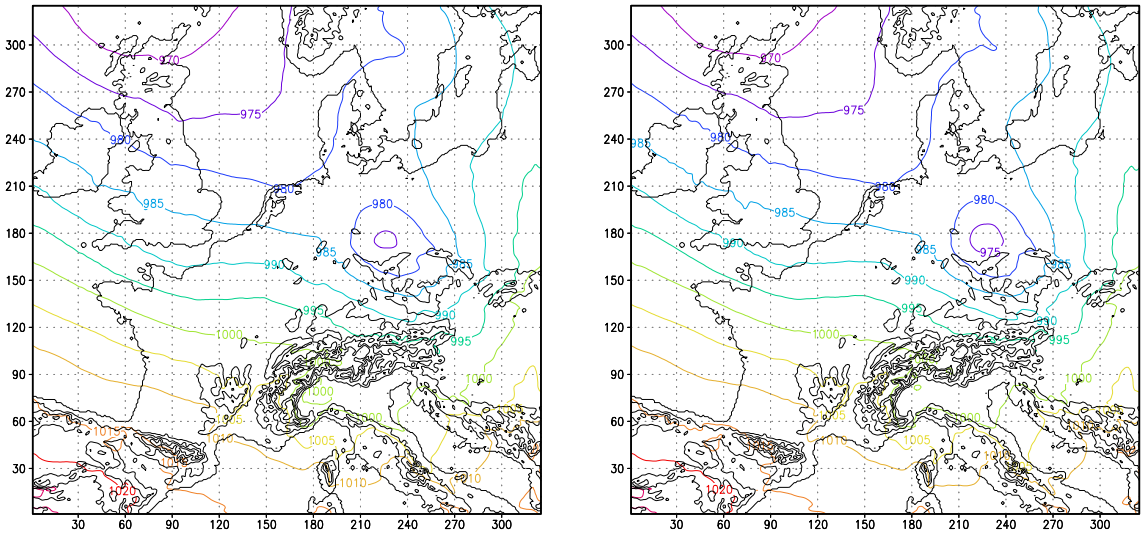

(a) Leapfrog / CD-2nd – $\Delta t = 40$ s.

(b) TVD-RK-3rd / UP-5th – $\Delta t = 72$ s.

Figure 2: *Winter storm "Lothar": 28 hour forecast of the mean sea level pressure in hPa for 26 December 1999, 16 UTC.*

References

Durran, D. R. (1999). *Numerical Methods for Wave Equations in Geophysical Fluid Dynamics*. New York: Springer.

Liu, X.-D., S. Osher, and T. Chan (1994). Weighted essentially non-oscillatory schemes. *J. Comput. Phys. 115*, 200–212.

Wicker, L. J. and W. C. Skamarock (2002). Time-splitting methods for elastic models using forward time schemes. *Mon. Wea. Rev. 130*, 2088–2097.

SPECTRAL ANALYSIS OF REAL-VALUED FUNCTIONS ON A SPHERE: VISUALIZATION OF SPATIAL SPECTRA

Alexander V. Frolov,
Roshydromet, Russia, afrolov@mecom.ru

An expansion of real functions in double Fourier series using associated Chebyshev polynomials was proposed in [1]. This expansion, in contrast to the traditional one based on spherical harmonics, is uniformly convergent on the globe, including the poles, and allows the use of Fast Fourier Transform in both directions [1, 2].

The associated Chebyshev polynomials of the first kind are simply depending on latitude. They can be expressed as Fourier series in terms of cosine polynomials for even zonal wave numbers *m* and as Fourier series in terms of sine polynomials for odd zonal wave numbers *m* [1]. Thus, the spatial spectrum of any real–valued function has a clear physical meaning; in particular, it can easily be visualized on a plane.

Let a real-valued function $f(\theta, \lambda)$ be defined on the surface of a sphere Ω ($0 \le \theta \le \pi$, $0 \le \lambda \le 2\pi$) and its square be integrable with some weight, i.e., $f(\theta, \lambda) \in L_2(\Omega)$. The function $f(\theta,\lambda) \in L_2(\Omega)$ is represented in the form of a double Fourier series:

$$f(\lambda,\theta) = \sum_n \left[d_n(\theta)\cos(n\lambda) + b_n(\theta)\sin(n\lambda) \right], \; b_0(\theta) \equiv 0. \tag{1}$$

The Fourier coefficients $d_n(\theta)$ and $b_n(\theta)$ are continuous functions of θ and can be uniformly fit by associated Chebyshev polynomials ($m=0,1$). Furthermore, we make the following transformation of (1):

$$\begin{gathered} f(\lambda,\theta) = \sum_n \left[d_n(\theta)\cos(n\lambda) + b_n \sin(n\lambda) = \sum_n C_n(\theta)\cos(n\lambda - \eta_n(\theta)) \right], \\ C_n(\theta) = \sqrt{d_n^2(\theta) + b_n^2(\theta)}, \;\; \eta_n(\theta) = sign(b_n(\theta)) ar\cos\left(d_n(\theta) \Big/ C_n(\theta) \right), \end{gathered} \tag{2}$$

where the amplitude $C_n(\theta)$ and the phase $\eta_n(\theta)$ are also continuous functions of θ and therefore can be expanded in Fourier series based on associated Chebyshev polynomials ($m=0,1$).
The appropriate Fourier series are

$$\begin{gathered} C_n(\theta) = \sum_m B_{n,m}\cos(m\theta), \quad \eta_n(\theta) = \sum_m \left(W'_{n,m}\cos(m\theta) + W''_{n,m}\sin(m\theta) \right), \\ C_n(\theta) = \sum_m A_{n,m}\cos(m\theta + \delta_m), \quad A_{n,m} = |B_{n,m}|, \;\; \delta_m = \frac{1 - sign(A_{n,m})}{2}\pi. \end{gathered} \tag{3}$$

Then instead of (1) we have

$$f(\lambda,\theta) = \sum_m \sum_n A_{n,m} \cos\left(n\lambda + \sum_m \left(W'_{n,m}\cos(m\theta) + W''_{n,m}\sin(m\theta) \right) \right). \tag{4}$$

As an example, we consider the spectrum of the 500 hPa geopotential height $H_{500}(\theta,\lambda)$. Eliminating the «climatic» component of $H_{500}(\theta,\lambda)$,

$$H'_{500}(\theta,\lambda) = H_{500}(\theta,\lambda) - \frac{1}{2\pi}\int_0^{2\pi} H_{500}(\theta,\lambda)\, d\lambda \;, \tag{5}$$

we can calculate the spatial spectrum of $H'_{500}(\theta,\lambda)$) by using (3), (4). The values of $A_{n,m}$ are shown in Fig. 1. Two power maximums corresponding to global $(m=n=1-3)$ and synoptic $(m=n=4-8)$ scales of the atmospheric circulation can be seen in the figure. The existence of these spikes is well known in meteorology, however, for the first time they were presented in such an obvious and pictorial form.

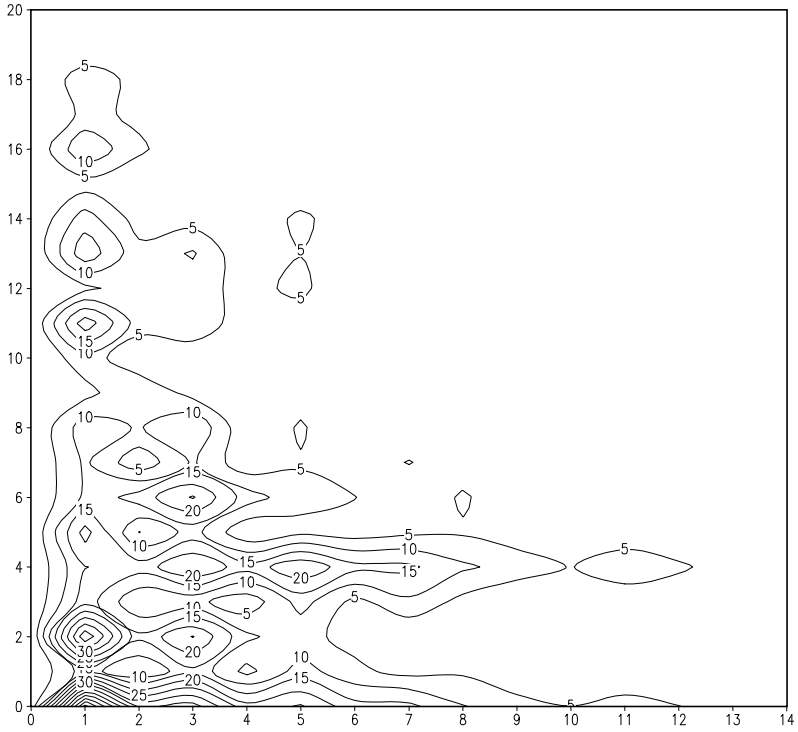

Figure 1. Distribution of amplitudes $A_{n,m}$ of 500 hPa geopotential height deviations $H'_{500}(\theta,\lambda)$ at $m=0,1,...,20$ (abscissa) and at $n=0,1,...,20$ (ordinate).

Following the same method, the spatial spectrum of any real-valued function can be constructed in any latitude belt or even in a spherical trapezoid.

REFERENCES

1. ***Frolov, A.V. and Tsvetkov, V.I., On harmonic analyses of real-valued functions on a sphere, – Submitted to the Journal of Numerical Mathematics and Mathematical Physics, December 2003.***

2. ***Tsvetkov, V.I., Fast algorithm for harmonic analysis of real-valued functions on a sphere (this report).***

Development of a 20 km mesh global NWP model on the Earth Simulator

Keiichi Katayama*, Hiromasa Yoshimura** and Takayuki Matsumura*
*Numerical Prediction Division, Japan Meteorological Agency
**Climate Research Department, Meteorological Research Institute
e-mail: k-katayama@naps.kishou.go.jp

1) Introduction

The global modeling groups of NPD/JMA and the Climate Research Department of MRI/JMA have been developing a very high resolution global model GSM-TL959L60 on the Earth Simulator (ES) (Katayama et al., 2003). The GSM-TL959L60 is a 20 km mesh global spectral model and adopts a new semi-Lagrangian scheme (Yoshimura et al., 2003).

We have optimized the model on the ES, and the execution time of 1-month forecast is about 3.5 hours using 60 nodes of the ES. We have executed several experiments of short range (3-5 days) and long range (1-2 years) forecasts, and the various meteorological phenomena such as typhoons and the Baiu fronts were well reproduced.

We will improve the computational performance and the physical parameterizations of the model in 2004. The GSM-TL959L60 will become operational on the next JMA supercomputer system in 2007.

2) Computational performance

We have optimized the model on the ES. Especially, the Legendre transform is well optimized with the vectorized matrix library. The message passing among the parallel nodes is also well optimized with the one-sided communication of MPI-2. Figure 1 shows a scalability of the GSM-TL959L60 on the ES. The computational performance of parallel calculation is very well from 12 nodes to 60 nodes. The computing efficiency with 60 nodes of the ES is about 35% of the peak performance.

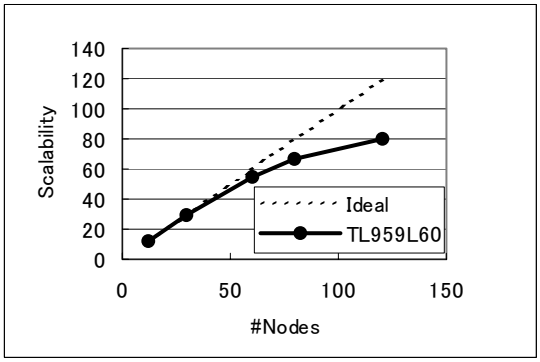

Fig.1 Scalability performance of the GSM-TL959L60 on the ES.

3) Forecast example of low temperature at Tokyo

It was a very cold summer in the eastern part of Japan in 2003. The surface temperature at Tokyo was very low in August 2003. It was not forecasted well with the operational NWP models.

We executed the forecast experiment with the initial field at that time. Figures 2 and 3 show the 5-days forecasts by the operational GSM-T213L40 and the GSM-TL959L60 on the ES. The low temperature at Tokyo was well reproduced in the 20 km mesh GSM-TL959L60. The GSM-TL959L60 also reproduced the blocking pattern in the east of Japan at 500 hPa height.

References

Katayama, K., H. Yoshimura and T. Matsumura, 2003: Development of a 20 km mesh global NWP model on the Earth Simulator. Research Activities in Atmospheric and Ocean Modeling, CAS/JSC Working Group on Numerical Experimentation, 33, 0311-0312.

Yoshimura, H., T. Matsumura, 2003: A Semi-Lagrangian Scheme Conservative in the Vertical Direction. Research Activities in Atmospheric and Ocean Modeling, CAS/JSC Working Group on Numerical Experimentation, 33, 0319-0320.

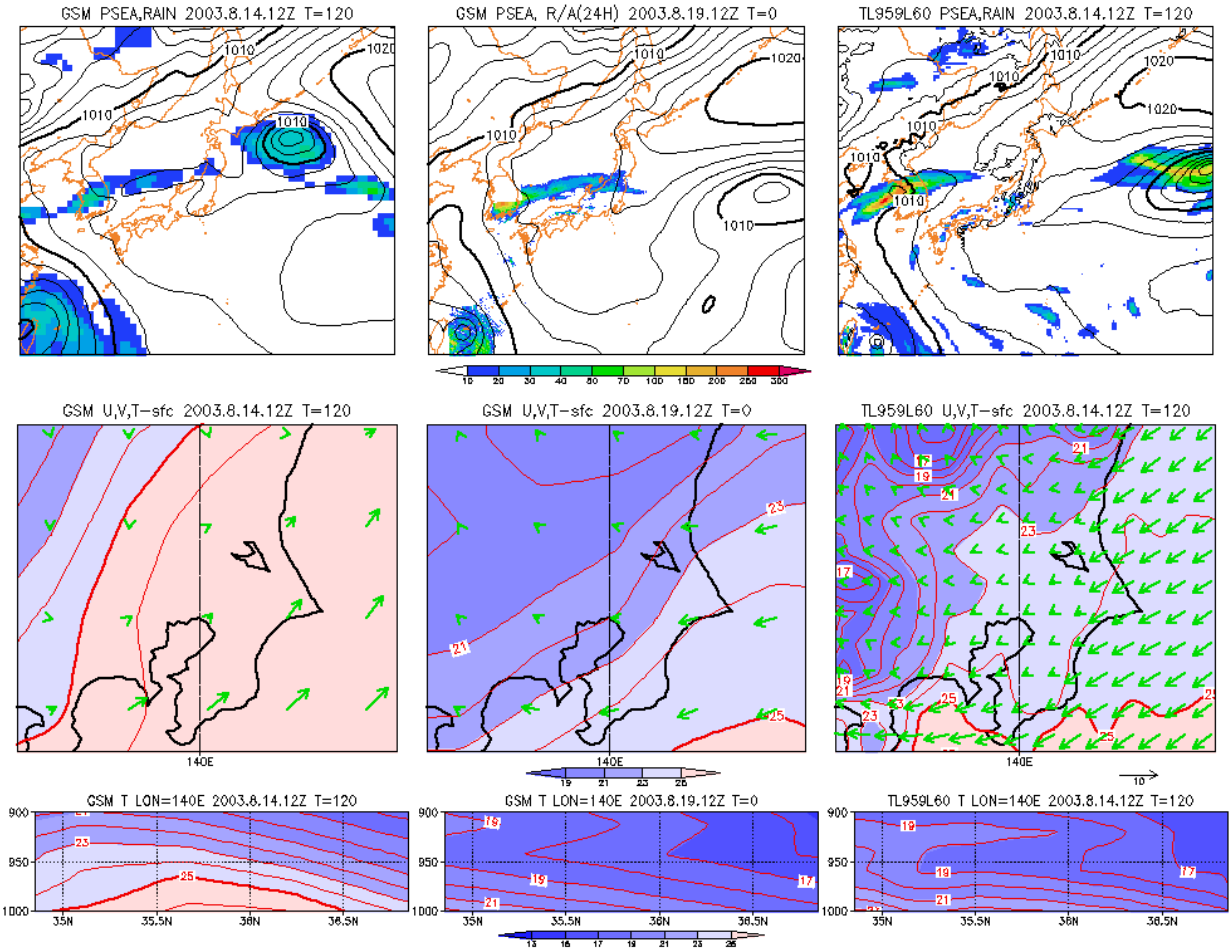

Fig.2 Forecast example of low temperature at Tokyo. GSM-T213L40 (left), global analysis and radar observation by JMA (center), GSM-TL959L60 (right). Psea and 24 hours precipitation (upper), surface temperature and wind (middle), vertical profile of temperature field in the lower atmosphere along 140E (lower).

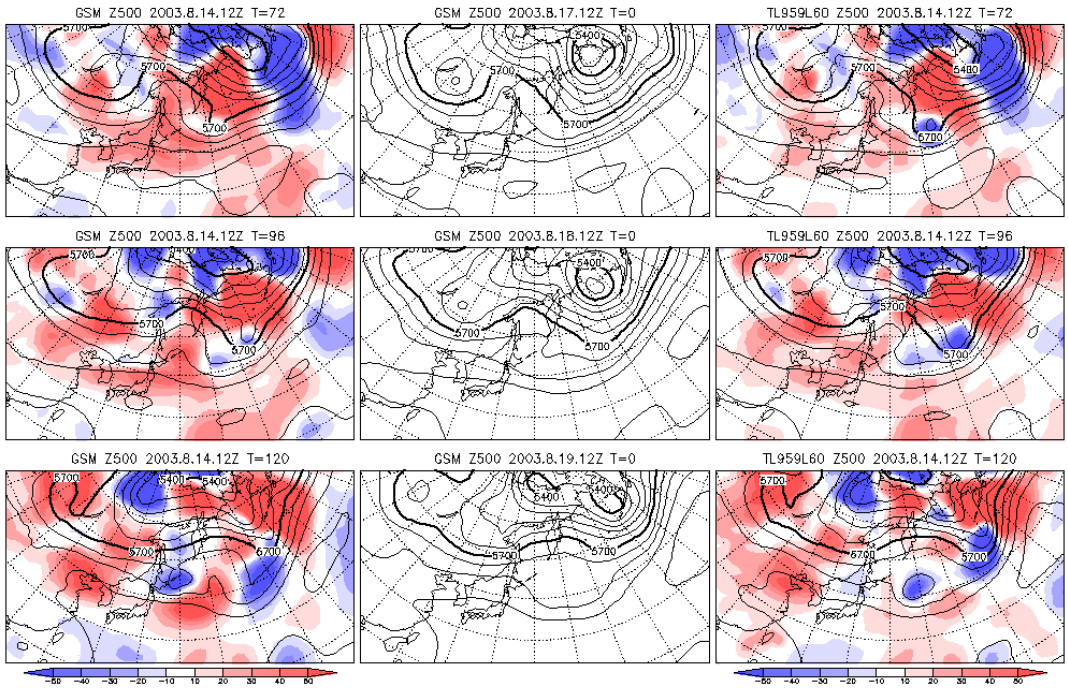

Fig.3 Forecasts of 500 hPa height field. GSM-T213L40 (left), global analysis (center), GSM-TL959L60 (right). Forecast times are 72 (upper), 96 (middle), and 120 hours (lower).

A COMPARISON OF SUPER-MATSUNO SCHEME AND DIGITAL FILTERING INITIALIZATIONS IN THE ETA MODEL

Lazar Lazic
Department of Meteorology, University of Belgrade, Serbia (lazar@ff.bg.ac.yu)

An iterative Matsuno or a "super-Matsuno" style scheme and digital filtering are applied as a filters in the Eta Model. The both initialization techniques are applied for the model's adiabatic part only. We are focusing on the impact of the use of initialization methods in a short-range forecasting environment/time-scale.

The super-Matsuno scheme (Fox-Rabinovitz, 1996) is a generalization of the Euler backward (Matsuno) scheme (Matsuno, 1966), to include more than one corrector step, that is, to include additional corrector iterations. Applying this scheme for the adjustment process in the Eta Model (Lazic, 2000), along with the backward scheme for the Coriolis terms, we have

- predictor:

$$\begin{aligned} u_*^{n+1} &= u^n - \Delta t g \delta_x h^n + \Delta t f v_*^{n+1} \\ v_*^{n+1} &= v^n - \Delta t g \delta_y h^n - \Delta t f u_*^{n+1} \\ h_*^{n+1} &= h^n - \Delta t H\left(\delta_x u + \delta_y v\right)^n \end{aligned} \tag{1}$$

- corrector:

$$\begin{aligned} u_1^{n+1} &= u^n - \Delta t g \delta_x h_*^{n+1} + \Delta t f v_1^{n+1} \\ v_1^{n+1} &= v^n - \Delta t g \delta_y h_*^{n+1} - \Delta t f u_1^{n+1} \\ h_1^{n+1} &= h^n - \Delta t H\left(\delta_x u_* + \delta_y v_*\right)^{n+1} \end{aligned}$$

along with *iterations of the corrector step*

$$\begin{aligned} u_2^{n+1} &= u^n - \Delta t g \delta_x h_1^{n+1} + \Delta t f v_2^{n+1} \\ v_2^{n+1} &= v^n - \Delta t g \delta_y h_1^{n+1} - \Delta t f u_2^{n+1} \\ h_2^{n+1} &= h^n - \Delta t H\left(\delta_x u_1 + \delta_y v_1\right)^{n+1} \\ &\cdots \\ u_k^{n+1} &= u^n - \Delta t g \delta_x h_{k-1}^{n+1} + \Delta t f v_k^{n+1} \\ v_k^{n+1} &= v^n - \Delta t g \delta_y h_{k-1}^{n+1} - \Delta t f u_k^{n+1} \\ h_k^{n+1} &= h^n - \Delta t H\left(\delta_x u_{k-1} + \delta_y v_{k-1}\right)^{n+1} \end{aligned} \tag{2}$$

where *k* is the *iteration number*. These corrector iterations can be continued until convergence takes place, namely, when

$$\| u_k^{n+1} - u_{k-1}^{n+1} \| < \varepsilon_1, \| v_k^{n+1} - v_{k-1}^{n+1} \| < \varepsilon_1, \| h_k^{n+1} - h_{k-1}^{n+1} \| < \varepsilon_2, \tag{3}$$

where ε_1 and ε_2 are prescribed small values and $\| \ \|$ is the maximum value norm.

This super-Matsuno-like time differencing scheme with iteration number *k=3* is applied to the adjustment stage of the Eta Model as an "initialization" procedure during the "*1h backward and +1h forward*" *adiabatic integration.*

Applying digital filter (Huang and Lynch, 1993) in the Eta Model an adiabatic integration is carried out backward in time for *N* time steps to produce a model state $X_d(n)$ at $t=-n\Delta t$. Here the *N*-step numerical integration covers half of the total filter span $T_s=2N\Delta t=4h$, which extends from $-N\Delta t$ to $+N\Delta t$. From *t=0*, the model then integrated forward in time to $+N\Delta t$, giving model variables $X_d(n)$ at $t=+n\Delta t$. The digital filter is then applied to $X_d(n)$, yielding a filtered field X_d^*

$$X_d^* = \sum_{n=-N}^{N} h(-n) X_d(n), \tag{4}$$

where *h(n)* are the filter coefficients

$$h(n) = \left\{ \frac{\sin[n\pi/(N+1)]}{n\pi/(N+1)} \right\} \frac{\sin\theta_c}{n\pi}. \tag{5}$$

Here θ_c is the cutoff digital frequency, which is related to the cutoff period $\tau_c = \pi T_s / N\theta_c$.

Initial conditions for a sensitivity experiment we ran are those of 0000 UTC 18 January 1987, selected in an earlier study for their featuring the tropical cyclones *Connie* and *Irma* from the Australian Monsoon Experiment (AMEX).

A common way to demonstrate the performance of an initialization scheme is to show the time evolution of the surface pressure and a midlevel vertical velocity at a model grid point. The surface pressure is sensitive to noise in a vertically integrated sense, while the midlevel vertical velocity indicates the internal noise.

The time evolution for the first 6 h of the forecast of the surface pressure p_s and 500 hPa vertical velocity $\omega = dp/dt$ at a model grid point I=25, J=18, without and with initialization, are shown in Fig. 1

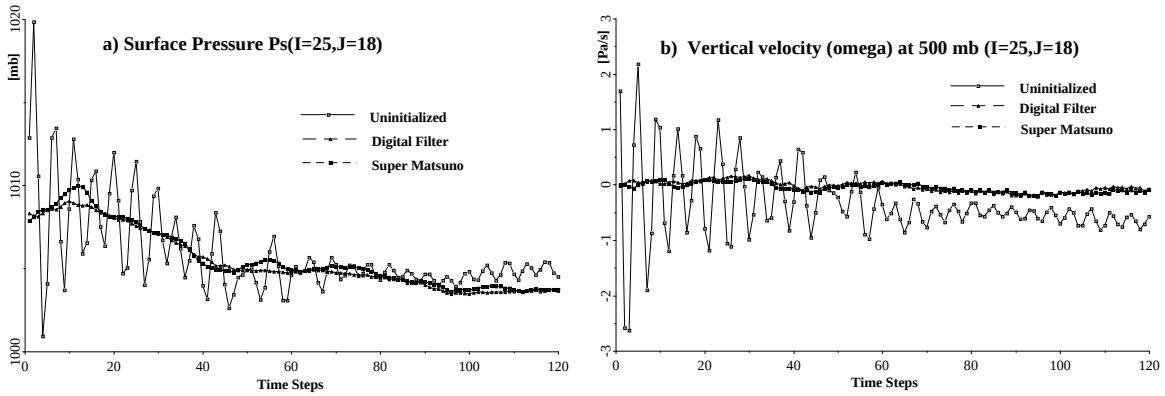

Fig. 1 Time evolution of: a) surface pressure p_s [hPa]; b) 500 hPa vertical velocity ω [Pa/s]; at a model grid point I=25, J=18, without and with initialization, during 6 h (120 time steps) of integration.

Uninitialized and initialized sea level pressure fields at the initial time are shown in Fig. 2. A high level of noise can be seen on uninitialized map, and no noise to be seen on initialized maps at the same time.

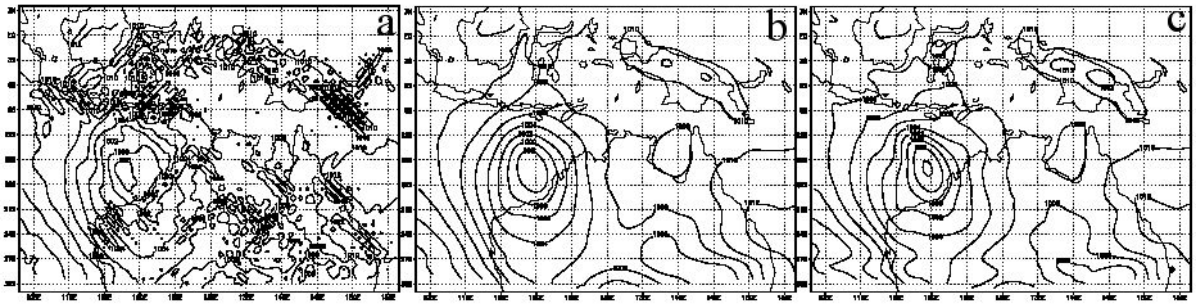

Fig. 2 Uninitialized (a), digital filter (b) super-Matsuno scheme (c) initialized sea level pressure [hPa]; at the initial time 0000 UTC 18 January 1987.

The super-Matsuno style time differencing scheme and digital filtering initializations remove the spurious high-frequency oscillations from the forecast *very efficiently*. After initializations fields are adjusted and without noise. It results in a lower noise level and a structure in the surface pressure tendency and 500 hPa vertical velocity at 1 h of integration significantly smoother than in the control case. In the control case fields still display a high level of noise.

The all integration results with and without initialization after 6 h are very similar. They are very similar also after 12 h and later until the end of the 48-h integration performed. Even so, it is to be expected that small differences, given that they have resulted from the removal of spurious initial noise have to be beneficial.

References

Fox-Rabinovitz, M.S., 1996: Diabatic dynamic initialization with an iterative time integration scheme as a filter. *Mon. Wea. Rev.*, **124**, 1544-1557.

Huang, X., and P. Lynch, 1993: Diabatic digital-filtering initialization: Application to the HIRLAM model. *Mon. Wea. Rev.*, **121**, 589-603.

Lazic, L., 2000: "Initialization" using an iterative Matsuno style scheme in the Eta Model adjustment stage. *Meteor. Atmos. Phys.*, **75**, 121-130.

Matsuno, T., 1966: Numerical integrations of the primitive equations by simulated backward difference scheme. *J. Meteor. Soc. Japan*, **44**, 76-84.

Conservative Semi-Implicit Semi-Lagrangian Method (CSSL) for Transport in Climate and Chemical Models

Ahmed Mahidjiba[(1)] and Jean Côté[(2)]
(1) Département des Sciences de la Terre et de l'Atmosphère, UQÀM, Montréal
(2) RPN, Meteorological Service of Canada, Dorval, QC, Canada H9P 1J3

Abstract :

The primary objective of this study is to improve the accuracy of transport schemes in coupled chemistry atmosphere models. In the first part of this study, we reproduced the known classical cases of passive advection in Cartesian geometry with both unstaggered (A-Grid) and staggered (C-Grid) grids. A series of 2D validations experiments were performed for 2D passive advection. These experiments have been done using idealized flow with known analytical solutions. Numerical results obtained are found to be in good agreement with analytical solution and those available in literature. In the second part of this study, we solved the full bidimensional equations of the shallow water model with constant Coriolis parameter. These governing equations were discretized by semi-Lagrangian and semi-implicit approach. This work represents the first step towords introducing conservative semi-Lagrangian transport in a shallow-water model.

1. Introduction

The first study concerning the semi-Lagrangian scheme seems to be due to André Robert (1982). Since then, this method has gained a wide acceptance in operational weather forecast and tracer transport models. The main advantages of this approach are its stability and good dispersion proprieties which, when combined with the semi-implicit or fully implicit discretization of the non-advective terms in weather forecast models, yields very robust and efficient yet accurate models. For a complete review of this method and related issues, see Staniforth and Côté (1991). The common problem with the semi-Lagrangian method is the lack of formal conservation of quantities, such as mass, due to interpolation. In fact, the lack of conservation of the semi-Lagrangian method may be a serious problem for climate studies, where many thousands of time steps are needed (long simulations). In applications such as the chemical transport of reacting species by the atmospheric circulation, it is important to ensure that the densities remain positive, and that no spurious sources and sinks are introduced by the transport process, since this could disturb the delicate non-linear chemical balance equations.

Several studies have been devoted to improve this aspect of the method. Such studies can be grouped in two principal categories. The first one concerns shape-preservation, which will guarantee positivity and global conservation either by simple renormalization or with an ingenious combination of low- and high-order interpolations. Both methods have been implemented successfully in semi-Lagrangian schemes. These corrective procedures were developed first by Priestly (1993). His quasi-conservative algorithm consists in restoring the desired quantity whilst minimizing changes to the original solution. The second category concerns the inherently-conservative semi-Lagrangian schemes. It consists in treating the local conservation where the total amount inside a material surface is constant. This type of conservation is relatively expensive and much more difficult to obtain. There is a family of methods similar to the semi-Lagrangian method that enjoys formal conservation at the local level. The most elegant algorithm was developed by Laprise and Plante (1995) for 1D problem. It should be noted that a computationally efficient implementation of these algorithms to higher dimensions is not a simple task. The extension to 3D problem, for example, requires a complex re-mapping which quickly becomes impractical for advective Courant numbers larger than one. Another approach that could be viable in 3D and at large Courant numbers and give local conservation is the use of the so-called cascade interpolation technique in combination with this re-mapping. Rancic (1995) has developed such a scheme for passive advection. His method consists of a natural extension to 2D of a 1D mapping and employs a bi-parabolic piecewise representation. Recently, Zerroukat and al. (2002) developed a Semi-Lagrangian Inherently Conserving and Efficient (SLICE) scheme based on a Control-Volume (CV) approach. The

Corresponding author address: Dr. Ahmed Mahidjiba, Ouranos, 550 Sherbrooke West Street, 19th floor, Montreal, QC, H3A 1B9, Canada. E-Mail: mahidjiba.ahmed.@ouranos.ca.

algorithm developed by those authors uses multiple sweeps of a 1D conservative remapping algorithm along pre-determined cascade directions and was tested for 2D standard passive advection.

As mentioned above, the major task of this work is to cure the problem of local conservation. In fact, we will be examining the feasibility of optimally combining these ideas for the development of an in-line transport model which will be efficient, conservative, shape-preserving, and applicable to non-hydrostatic models as well. The main purpose of the paper is to describe the principal parts of this investigation realized until now. Validation results of 2D passive advection using the semi-Lagrangian schemes based on the Arakawa C-Grid in Cartesian frame are shown in this paper.

2. The preliminary results: Passive advection

In the first stage, the numerical model was validated for the 2D prognostic equation of passive advection given by:

$$\frac{dF}{dt} = \frac{\partial F}{\partial t} + u\frac{\partial F}{\partial x} + v\frac{\partial F}{\partial y} = 0 \qquad (1)$$

where the function $F(x,y,t)$ stands for any physical variables characterizing the atmosphere.

The first test consists of the classical idealized cyclognesis case defined by an initial circular vortex with a tangential velocity. Only the results will be presented here (see, *Zerroukat et al. (2002) for details). All results have been obtained for the set of parameters:* $\Omega = [0 \quad 10\,m]^2$, $N_x = N_y = 129$, $N_t = 16$, $\Delta t = 0.3125\ [s]$, $V_{\max} = 2.5981\ [m/s]$.

The error measure is defined as the root-mean-square (*RMS*) difference between the analytical solution and the numerical one with the departure point calculated numerically or analytically.

Table 1 shows the results obtained for the cyclognesis problem. These results are compared with those obtained analytically and available in literature (Zerroukat et al (2002)).

Figure 1 shows the results obtained with the two grids for the classical idealized cyclognesis case described above. These results show the variation of *RMS* as function of time. We note that the analytical solution obtained by Zerroukat et al. (2002) is completely reproduced.

Table 1: Idealized cyclognesis problem results

		Error : RMS	
Work	**Grid**	**Analytical**	**Numerical**
Zerroukat et al (2002).	A-Grid	0.074217	Not available
	C-Grid	Not available	Not available
Present work	A-Grid	**0.074217**	**0.082840**
	C-Grid	**0.074217**	**0.081407**

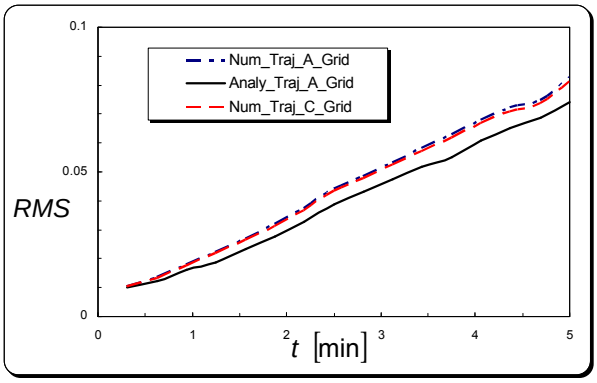

Fig. 1: The variation of root-mean-square, *RMS* as a function of time t [min]

References

Laprise, R. and Plante, A., 1995, A class of semi-Lagrangian integrated mass (SLIM) numerical transport algorithms, *Mon. Wea. Rev*., **123**, 553-565.

Priestley, A. 1993, A quasi-conservative version of the semi-Lagrangian advection scheme, *Mon. Wea. Rev*., **121**, 621-629.

Rancic, M. 1995, An efficient conservative monotonic remapping for semi-Lagrangian transport algorithms, *Mon. Wea. Rev*., **123**, 1213-1217.

Robert, A., 1982, A semi-Lagrangian and semi-implicit integration scheme for the primitive meteorological equations. *Jpn. Meteor. Soc.*, **60**, 319-325.

Staniforth, A. and J. Côté, 1991, Semi-Lagrangian integration schemes for atmosphere models- A review. *Mon. Wea. Rev*., **119**, 2206-2223.

Zerroukat, M., Wood, N. and Staniforth A., 2002, SLICE: A Semi-Lagrangian Inherently Conserving and Efficient scheme for transport problems, *Q. J. R. Meteorol. Soc*. **128**, 2801-2820.

Vertical resolution impacts on modeled Gulf of Mexico Loop Current Eddies

Steven L. Morey and James J. O'Brien

Center for Ocean – Atmospheric Prediction Studies
Florida State University
Tallahassee, FL 32306-2840
morey@coaps.fsu.edu, obrien@coaps.fsu.edu

1. Introduction

This study examines the role vertical resolution plays in simulating the Loop Current Eddie (LCE) formation, propagation, and decay in an ocean model. It is quite possible that even the highest vertical resolution models published to date are not adequately resolving the large vertical gradients associated with the energetic Loop Current (LC) and LCEs, nor are adequately resolving near-bottom processes that may affect the upper ocean circulation. The impacts of vertical resolution are studied with the Navy Coastal Ocean Model (NCOM) configured to realistically simulate the GoM. Experiments are run with differing vertical resolutions and the eddy behavior in the solutions is examined.

Results suggest that higher vertical resolution simulations produce a more variable eddy field, and stronger LCEs. The propagation pathways appear more realistic compared to Topex/Poseidon satellite altimeter observations. In the lower vertical resolution simulation, LCEs tend to decay more preferentially in the northwestern corner of the GoM resulting in an unrealistically permanent anticyclone. This anticylonic feature is much weaker in the higher vertical resolution simulation.

2. The Model

The NCOM is a three-dimensional primitive equation hydrostatic ocean model developed at the Navy Research Laboratory [*Martin*, 2000]. The model's hybrid sigma (terrain following) and z (geopotential) level vertical coordinate is useful for simulating upper ocean processes in domains encompassing both deep ocean basins and very shallow shelves. The NCOM is set up to simulate the entire GoM and Caribbean north of Honduras (15.55°N) to 80.6°W with 1/20° between like variables on the C-grid, 20 sigma levels above 100 m and either 20 or 40 z-levels below 100 m to a maximum depth of 4000 m [*Morey et al.*, 2003]. The model is forced by discharge from 30 rivers, transport through the open boundary (with monthly climatology temperature and salinity) yielding a mean transport through the Yucatan Strait of approximately 27 Sv ($10^6 m^3 s^{-1}$), and monthly climatology surface heat and momentum flux. A surface salinity flux has the effect of uniformly evaporating an amount of water at a rate equal to the sum of the annual average discharge rates of the 30 rivers. The model is run for 10 years for each experiment, with the last seven years used for analysis.

3. Results

The variance of the model sea surface height (SSH) shows highest values in the region of the LC retroflection and LCE separation (Fig. 1). A region of high SSH values stretch westward from the LC across the GoM near the latitude band of 23°N to 28°N, showing the preferred westward propagation pathways of the shed LCEs. The 60 level experiment shows much larger values of the SSH variance, with a more pronounced maximum near the LC retroflection, and a less pronounced secondary maximum in the northwestern corner of the GoM than the 40 level experiment.

The mean SSH (surface deviation from a resting level) maps from the two GoM experiments both show a high in the northwestern corner of the GoM, indicating a preferred location for the anticyclonic LCEs to reside. The 40 level experiment has relative maxima here of over 30 cm, compared to less than 20 cm for the higher vertical resolution 60 layer experiment. The mean SSH scaled by the standard deviation is less than 1.0 in the 60 level experiment, indicating that the anticyclone is not a permanent feature at this location. However, in the 40 level experiment, the SSH mean scaled by the standard deviation is greater than 3.0 in the northwestern GoM suggesting a nearly permanent anticylonic feature exists here. Although an anticyclone is evident in the mean dynamic topography from historical data, observations do not support that this is a permanent feature. Thus, the higher vertical resolution experiment seems to simulate a more realistic eddy field in the western GoM.

The sea level variability across a line coincident with a Topex/Poseidon satellite altimeter (T/P) ground track is compared between NCOM GoM simulations and T/P data (Fig. 3). LCEs cross this track as they propagate westward from the Loop Current. The sea surface height variance versus latitude plot gives some indication of the eddy strength and preferred propagation path. The results show weaker than expected sea level variability across this track in the 40 level experiment, and much better agreement in the near-twin experiment with 60 vertical levels.

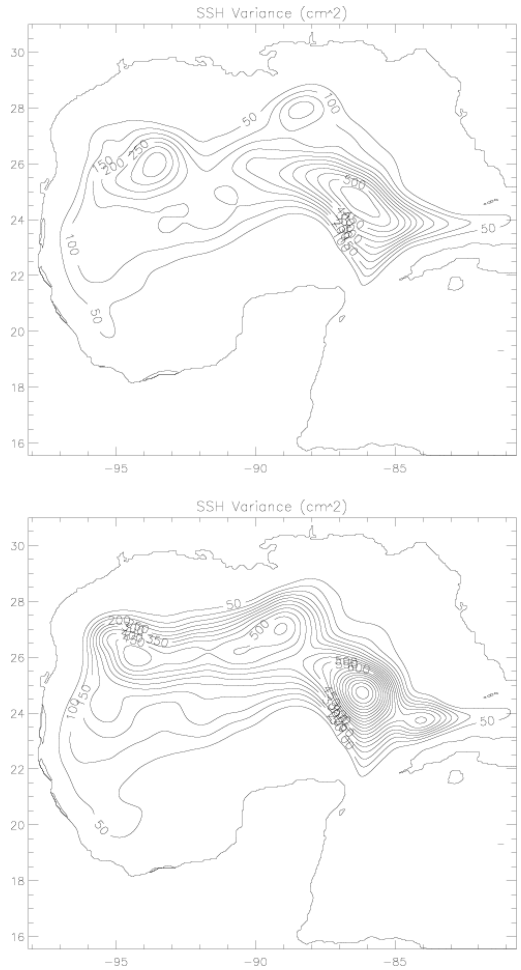

Fig. 1. Variance (cm^2) of the model SSH from the 40 level experiment (top) and the 60 level experiment (bottom). The contour interval is 50 cm^2.

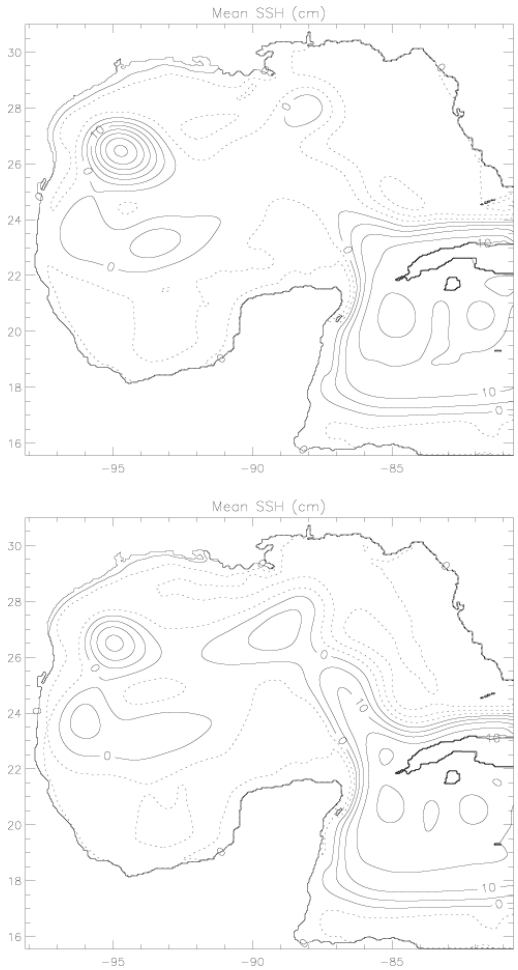

Fig. 2. Model mean SSH (cm) from the 40 level experiment (top) and the 60 level experiment (bottom). The contour interval is 5 cm and negative values are indicated by dotted contour lines.

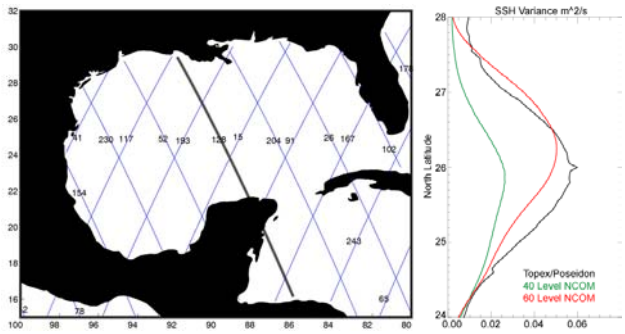

Fig. 3. Right: Variance of the sea surface height versus latitude for seven years of data across T/P ground track 128 shown highlighted at left. Black curve: Topex/Poseidon altimeter. Green curve: 40 level simulation. Red curve: 60 level simulation.

Acknowledgements

The authors wish to thank Paul Martin and Alan Wallcraft at the Naval Research Laboratory for development of the NCOM. This project was sponsored by the Office of Naval Research Secretary of the Navy grant awarded to James J. O'Brien, and by a NASA Office of Earth Science grant to the COAPS authors. Computer time was provided by the FSU School of Computational Science and Information Technology and by the Department of Defense High Performance Computing Modernization Program. Thanks also to Jorge Zavala for his contributions.

References

Martin, P., *A Description of the Navy Coastal Ocean Model Version 1.0.* NRL Report NRL/FR/7322-009962, Navy Research Laboratory, Stennis Space Center, MS, 2000.

Morey, S.L., P. J. Martin, J. J. O'Brien, A. A. Wallcraft, and J. Zavala-Hidalgo, Export pathways for river discharged fresh water in the northern Gulf of Mexico, *J. Geophys. Res., 108*(C10), 3303, doi:10.1029/2002JC001674, 2003.

AGCM parallel algorithm development for cluster computers

V.P. Parkhomenko, A.V. Shipilin, S.A. Zabelok

Computing Centre of the Russia Academy of Sciences

Vavilov Str. 40 Moscow 119967 Russian Federation

E-mail: parhom@ccas.ru

Computing Centre (CC) AGCM uses uniform 72 degrees on longitude and 46 degrees on a latitude horizontal grid for single processor computer. Program was modified for high performance cluster.

Global area was distributed between processors (domain decomposition) on meridians at parallel version of the program.

Advantage of this way is that all this geographic areas are similar, and the same algorithm of calculations can be used on all processors. Lack of this approach is that each of areas borders on all by others (in points of northern and southern poles). It results that the data on the previous temporary layer are necessary for receiving for calculations of points near to poles from all other processors, that assumes enough amount of information interchanges between processors.

The information interchanges between processors on each time layer (sublayer) are necessary only at performance advective steps. All areas are identical with the computing point of view, and the amount of the information, transmitted between processors, is not great, namely, those parts of numerical arrays are transferred only which correspond to boundary points of subareas. It provides high efficiency of algorithm.

The library MPI was used as a means of parallel program realization.

The opportunity of splitting on various number of subareas is stipulated in parallel variant of the program, depending on quantity of the involved processors. The data received on the single processor computer are used as initial. The converter program is created for compatibility with the available data.

The basic properties of the given parallel program briefly can be formulated as follows:

1. Amount of duplicated operations is small, because all calculations will be carried out independently, and the group operations are effectively realized by means MPI.

2. Loading on processors is balanced, as the area is divided into subareas identical each other.

3. Time of is small, as the volumes of the information, sent at exchanges, are small, and the time of calculations between exchanges is rather great.

4. The memory of processors is used effectively, as the basic volumes of the information - file of results and all preliminary files - are allocated on processors.

The test calculations on high-efficiency Computer Center cluster. (2 - 8 processors) are carried out. The good agree of results for single processor and parallel programs is received. The comparison of times of calculations has shown (fig. 1), that on 4 processors the acceleration at 3.81 times is received in comparison with the single processor program. It corresponds to efficiency 95 %, that allows to make a conclusion about the good parallel characteristics of the developed program.

It is necessary to study other ways of considered area splitting: splitting along geographical parallels, and splitting combining both ways. Also it is necessary to provide an

opportunity of transition to more detailed grids, that is required for coupling of regional models with global.

This work is supported by RFFI.

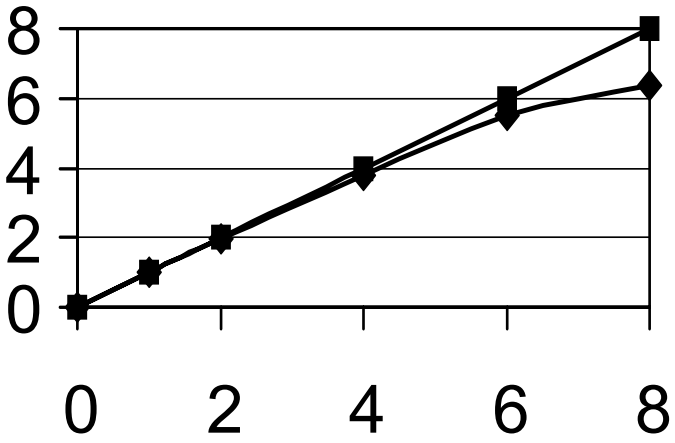

Figure 1. Dependence of run acceleration (lower line) from processors numbers (horizontal axes)

Tests of a Z-Coordinate Nonhydrostatic Model Including Physical Processes

J. Steppeler, S. Janjic**, H. W. Bitzer***, P. Prohl*, U. Schättler**
*DWD , **NCEP,***AWGeophys
Offenbach, Frankfurterstr. 135

Z-Coordinate numerical models of the atmosphere have the advantage of representing the atmosphere at rest properly and therefore justify the expectation of improved forecasts of orographically induced winds. An example for such a Z-coordinate model is the etamodel, which is based on the step orography. The step approach does not allow for a proper representation of the meso-scale flow over smooth and well resolved mountains. This problem was pointed out by Gallus and Klemp (2000). Steppeler et al (2002a) showed that the problem can be solved by formulating lower boundaries using a representation of the mountains by linear splines rather than the step approach. On this basis a Z-coordiante version of the model LM (see Steppeler et al. (2002b)) was developed and tested extensively in idealised situations using bell shaped mountains and the orography of Scandinavia.

A physical parameterisation package was created by using the parameterization package for the terrain following model LM and developing an interface between the z-levels and the terrain following levels. The tendencies of the physics routine in the terrain following grid are interpolated by cubic splines to the z-representation.

A number of idealised tests were done. A bell shaped mountain of height 2000 m was used with an atmosphere being initially at rest. Different circulations developed at night and day, corresponding to mountain and valley winds. In comparison, the model version using terrain following coordinates produced a mountain wind even without radiation being switched on. When a homogeneous velocity field of 10 m/sec is used with the same mountain, a warming or cooling is produced in the wake of the mountain, leading to a rotational motion perpendicular to the axis of the main motion. With radiation switched off the temperature in the wake of the mountain is unchanged.

Fig. 1 shows a test where the step type z-coordinates had a disadvantage as compared to terrain coordinate models. A shallow mountain of 400 m height is used with a homogeneous velocity field of 10 m/sec. The cloud water field in a vertical cross section through the centre of the mountain and the precipitation field is shown. Due to the proper treatment of the gravitational wave, these results come out in the expected way.

References:

Gallus, W. and J. Klemp, 2000: Behaviour of flow over step orography. *Mon. Wea. Rev.* ***128****, 1153-1164.*

Steppeler, J. , H. W. Bitzer, M. Minotte, L. Bonaventura, 2002a: Nonhydrostatic Atmospheric Modelling Using a z-Coordinate Representation. *Mon. Wea. Rev* ***130****, 2143-2149.*

Steppeler, J., G. Doms, U. Schättler, H. W. Bitzer, A. Gassmann, U. Damrath, G. Gregoric, 2002b: Meso-gamma scale forecasts using the nonhydrostatic model LM, *MAP* ***82****, 75-96.*

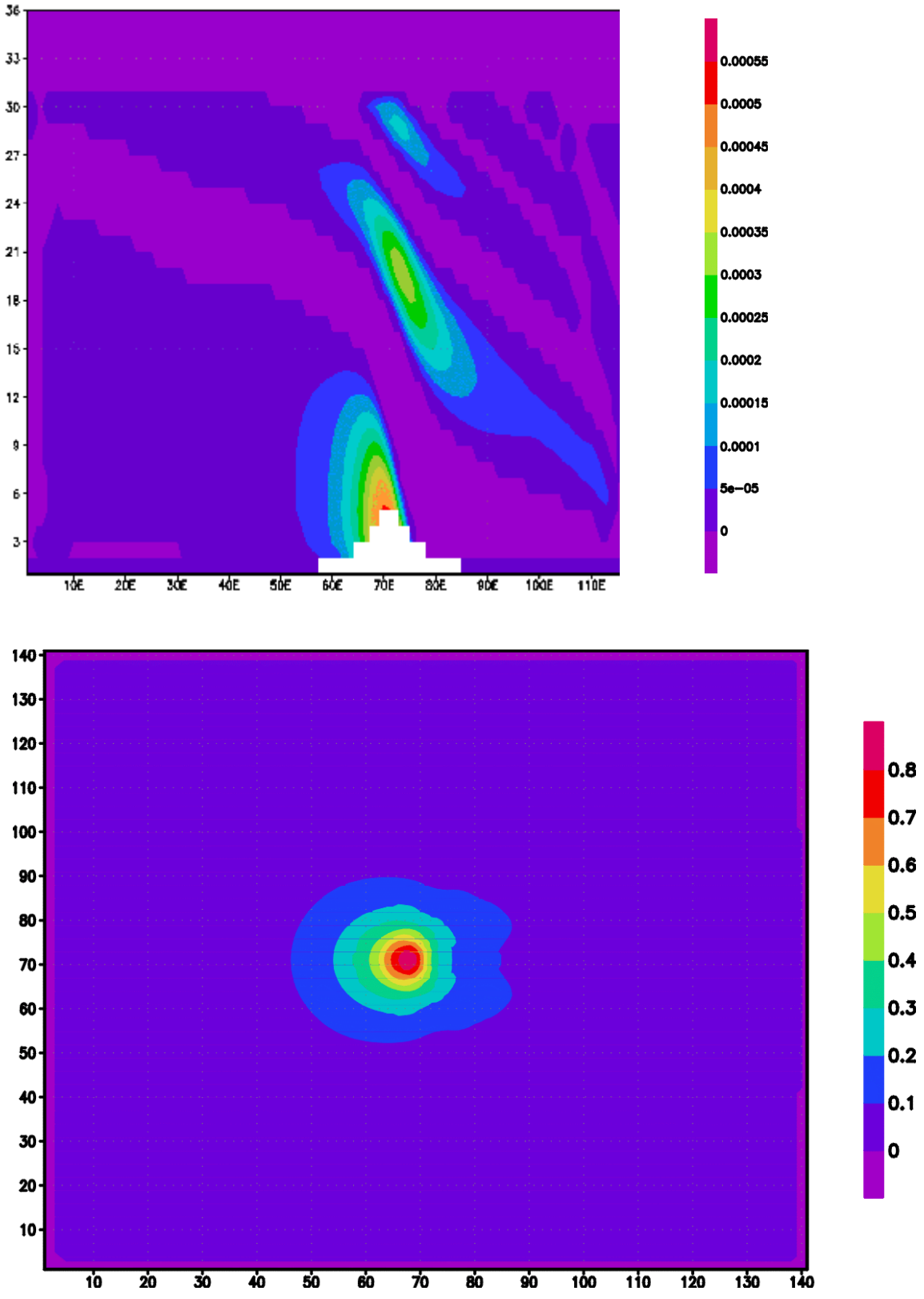

Fig. 1: Cloud water (kg/kg) on a cross section through the centre of the mountain (top) and precipitation (mm) for the bell shaped mountain of height 400 m in a homogeneous velocity field.

FAST ALGORITHM OF HARMONIC ANALYSIS OF REAL-VALUED FUNCTIONS ON A SPHERE

Vyacheslav I. Tsvetkov,

Hydrometeorological Center of Russia, tsvetkov@rhmc.mecom.ru

Let us consider a sphere of unit radius centered at the origin. Let us take the coordinate system using the following independent variables: co-latitude θ ($\theta = \pi/2 - \varphi$, where φ is the latitude), longitude λ, and radial coordinate ρ. We introduce the notation $x = \cos\theta$.

Let us consider the Jacobi polynomials on the interval [-1, 1]. They are orthogonal with a weight function $h(x) = (1- x)^{\alpha}(1+ x)^{\beta}$ ($\alpha > -1$, $\beta > -1$) [1,2]. The integrability of function $h(x)$ is provided by the conditions $\alpha > -1$, $\beta > -1$.

At $\alpha = \beta$ the Jacobi polynomials $P_n^{(\alpha,\alpha)}(x)$ turn into the so-called ultraspherical polynomials [2], which satisfy the hypergeometric equation

$$\left(1 - x^2\right)y'' - 2(\alpha + 1)xy' + n(n + 2\alpha + 1)y = 0\,. \qquad (1)$$

In this case, the weight function $h(x)$ is even and the ultraspherical polinomials $P_n^{(\alpha,\alpha)}(x)$ will be even or odd depending on eveness or oddness of its order n, that is, $P_n^{(\alpha,\alpha)}(x) = (-1)^n P_n^{(\alpha,\alpha)}(-x)$.

Let $\alpha = \nu - 1/2$ ($\nu > -1/2$). According to [2], let us introduce the following notation and normalization:

$$P_n^{(\nu)}(x) = \frac{\Gamma(\alpha+1)}{\Gamma(2\alpha+1)}\frac{\Gamma(n+2\alpha+1)}{\Gamma(n+\alpha+1)}P_n^{(\alpha,\alpha)}(x) = \frac{\Gamma\left(\nu+\frac{1}{2}\right)}{\Gamma(2\nu)}\frac{\Gamma(n+2\nu)}{\Gamma\left(n+\nu+\frac{1}{2}\right)}P_n^{\left(\nu-\frac{1}{2},\nu-\frac{1}{2}\right)}(x). \qquad (2)$$

Note the following important particular cases of ultraspherical polynomials. The equation

$$\left(1 - x^2\right)T_n'' - xT_n' + n^2T_n = 0\,, \qquad (4)$$

follows from (2) at $\nu = 0$. Its solutions are the first kind Chebyshev polynomials $T_n(x) = P_n^{(0)}(x)$.

At $\nu = 1$ Eq. (2) reduces to the equation

$$\left(1 - x^2\right)U_n'' - 3xU_n' + n(n+2)U_n = 0\,, \qquad (5)$$

the solution of which are the second kind Chebyshev polynomials $U_n(x) = P_n^{(1)}(x)$. The third particular case at $\nu = 1/2$ gives the solution of Eq. (2), which is called the Legandre polynomials, $L_n(x) = P_n^{(1/2)}(x)$.

Note that $P_n^{(\nu)}(\cos\theta)$ can be represented in the form of the Fourier expansion in orthogonal first-kind Chebyshev polynomials [2]:

$$
\begin{aligned}
&P_n^{(0)}(\cos\theta) = \cos n\theta, \\
&P_n^{(\nu)}(\cos\theta) = 2\gamma_0\gamma_n \cos n\theta + 2\gamma_1\gamma_{n-1}\cos(n-2)\theta + \ldots \\
&\ldots + \begin{cases} 2\gamma_{(n-1)/2}\gamma_{(n+1)/2}\cos\theta & \text{for odd n} \\ \gamma_{n/2}^2 & \text{for even n} \end{cases}
\end{aligned}
\tag{3}
$$

where γ_n are the coefficients calculated by the following formulas

$$
\gamma_0 = 1, \quad \gamma_n = \binom{n+\nu-1}{n} = \frac{\nu(\nu+1)\ldots(n+\nu-1)}{n!}, \quad n = 1,2,..N; \quad \nu > 0
$$

It is easy to see that the first-kind Chebyshev polynomials are cosine polynomials. Hence, the associated Legandre functions can be expressed through the trigonometric polynomials. In this case, the real-valued function $f(\theta, \lambda)$, determined on the surface of a sphere Ω ($0 \le \theta \le \pi$, $0 \le \lambda \le 2\pi$) and integrable with some weight (that is, $f(\theta, \lambda) \in L_2(\Omega)$), can be expanded in Fourier series using the fast Fourier transformation algorithm [3]. When this algorithm is used to calculate the Fourier coefficients over latitude and over the whole globe, the number of arithmetic operations becomes as small as $O(N*lnN)$ and $0(N^2*lnN)$, respectively.

References

1. ***Hobson E*.W. The Theory of Spherical and Ellipsoidal Harmonics. Cambridge,1931.**
2. ***Gabor Szego.* Ortogonal polynomials. Publ. Amer. Math. Soc., 1959**
3. ***Frolov A.V. and V.I. Tsvetkov. "On harmonic analyses of real-valued functions on a sphere" – Submitted to the Journal of Numerical Mathematics and Mathematical Physics, December 2003 .***

An Isentropic Model of the Atmosphere

Tim Woollings and John Thuburn, University of Reading, UK
swr01tjw@met.rdg.ac.uk

The isentropic middle atmosphere model of Gregory (1999) has been extended down to the Earth's surface incorporating a new boundary formulation. The model is based on the shallow water model of Thuburn (1997) and predicts PV, divergence δ and isentropic density $\sigma = \rho\frac{\partial z}{\partial \theta}$ on a hexagonal-icosahedral horizontal grid with an isentropic vertical coordinate. Here we briefly describe the model, in particular the lower boundary formulation, and present some early results.

One of the major difficulties in isentropic modelling of the atmosphere is that the coordinate surfaces intersect the ground. In the past attempts to overcome this problem have been based upon two key techniques: the idea of using extrapolated underground values to calculate finite differences near the ground, and the massless layer approach whereby after hitting the ground an isentropic model layer is extended along the surface with negligible mass.

Our formulation could be considered as a combination of the two. We use a general vertical coordinate η which is equal to the potential temperature θ above ground (see figure 1). When a level hits the ground it retains the same coordinate value η. Two different density fields are then defined: σ is the standard isentropic density above ground and continues underground with non-zero values. $\hat{\sigma}$ is equal to σ everywhere above ground and goes to zero at the ground in the same way as in the massless layer method. Initial values for σ, as well as PV and δ, are extrapolated along isentropes from the surface. Both densities the evolve prognostically according to the mass conservation equation.

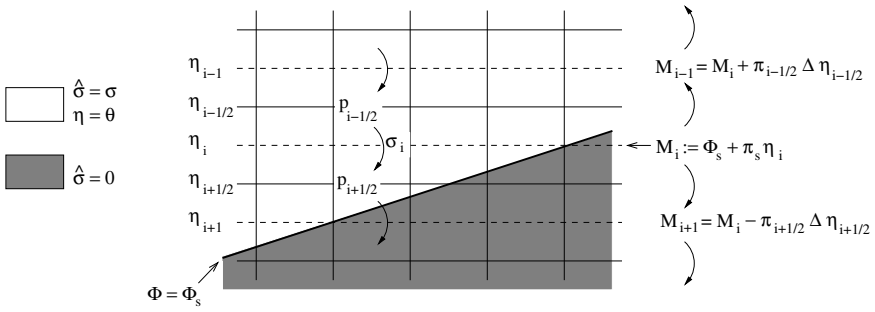

Figure 1: A schematic of the lower boundary scheme used in the model. The boundary condition is a specified geopotential Φ_s and the Montgomery potential M in the lowest massy level is calculated from this as shown for the furthest right column. The arrows indicate directions of integration. p is the pressure, $\pi = c_p\left(\frac{p}{p_0}\right)^{\kappa}$ and the other symbols are defined in the text.

The real atmosphere is therefore represented by the non-zero $\hat{\sigma}$ region and the underground values of σ are there simply as a numerical device used to represent the ground smoothly. This is done in an attempt to avoid another common problem with isentropic models, described by Randall (2000) and summarised here. In isentropic coordinates the horizontal pressure gradient force is the Laplacian of the Montgomery potential M and this is calculated by integrating the pressure up from the surface according to the hydrostatic equation $M_\theta = \pi(p)$. However with discrete isentropic levels intersecting the ground the surface θ distribution is not smooth leading to noise in M at all levels above an intersection point.

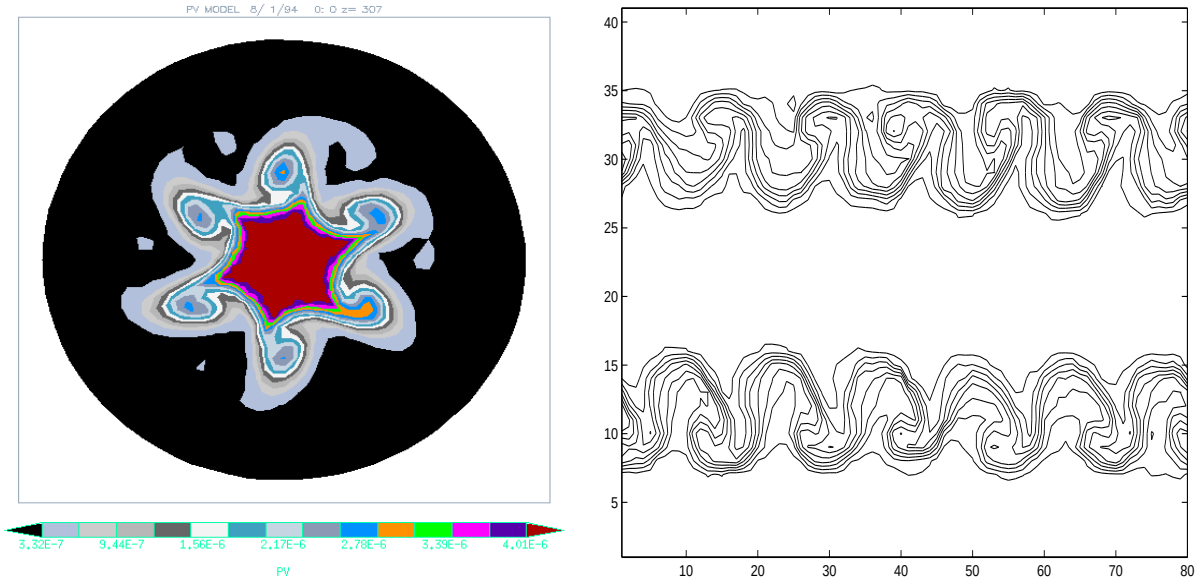

Figure 2: On the left Northern hemisphere PV on the 307K level at day 8 of the baroclinic wave and on the right the global surface θ at the same time. Horizontal resolution is equivalent to T50.

In our formulation we hope to solve this problem by using the underground σ values to interpolate vertically for the exact location of the ground in the η coordinate framework so that the surface temperature distribution is smoothly defined. This interpolation is implemented simply by defining M in the lowest massy level using the formula in Figure 1, and M at all levels is then calculated by integrating from here. Note that below ground both this integral and the integral of density to obtain pressure propagate information downwards. No information from below ground propagates upwards to contaminate the real above-ground flow. This however means that in the unphysical below ground region there is no gravity wave feedback mechanism and so the region is unstable. The region has no physical meaning and so the instability is controlled by simply relaxing the flow back towards the initial conditions in such a way that the surface winds are unchanged. The underground region provides for smooth interpolation of surface conditions and is carefully controlled so as to be stable and not to interfere with the real atmospheric flow.

The model has been run successfully in an adiabatic state on simulations such as the development of a baroclinic wave lifecycle as shown in Figure 2. However the model has had difficulty simulating the decay phase of the wave when θ surfaces become tightly packed at the surface front; in the future it is planned to introduce a simple representaion of diabatic processes in an attempt to improve this.

References

Gregory, A. (1999). *Numerical simulations of winter stratosphere dynamics.* Ph.D. thesis, University of Reading.

Randall, D. A., editor (2000). *General Circulation Model Development*, chapter 17. Academic Press.

Thuburn, J. (1997). *A PV-based shallow-water model on a hexagonal-icosahedral grid.* Monthly Weather Review, **125**, 2328-2347.

Implementation of the Cylindrical Equidistant Projection for the Non-Hydrostatic Model of the Japan Meteorological Agency

Yosuke Yamazaki[1] and Kazuo Saito[2]

[1]Advanced Earth Science & Technology Organization

[2]Numerical Prediction Division, Japan Meteorological Agency

e-mail: y-yamazaki@naps.kishou.go.jp

The Non-Hydrostatic Model (NHM) is a regional grid-point model which is based on the finite difference scheme and will replace current operational regional hydrostatic spectral model, the Mesoscale Spectral Model (MSM) of the Japan Meteorological Agency (JMA). Recently, the importance of developing non-hydrostatic global model has been increasing with the advance of the computer technology. One of the easiest ways to modify a grid-point model from a regional model to a global one is to implement the latitude-longitude (lat-lon) coordinate. Saito (2001)[1] made a global non-hydrostatic model by implementing the Cylindrical Equidistant (CE) projection for NHM together with a special treatment for the grid points near the poles. A preliminary 24 hours simulation with the horizontal resolution of 1.5 degrees for latitude and longitude was carried out for a global domain using the global analysis (GANAL) of JMA as the initial condition. Although the test run reproduced well the synoptic scale motions of the atmosphere, it would be difficult to perform simulations with higher horizontal resolution because the model was based on a previous version of NHM which was not parallelized. The implementation of the CE projection supported only the semi-implicit scheme (HI-VI scheme), which treats the fast modes (sound waves) implicitly in both horizontal and vertical directions.

The CE projection has been implemented again for the latest version of NHM, which is fully parallelized by using the MPI library and includes many new features such as the Kain-Fritsch cumulus parameterization and higher-order advection schemes[2]. The split-explicit scheme (HE-VI scheme) which treats the fast modes explicitly in the horizontal direction and implicitly in the vertical direction is also supported, together with a newly developed time-splitting scheme for advection terms[3].

NHM is designed to select a type of map projection by its runtime option, and have supported 3 conformal projections; the Polar Stereographic projection, the Lambert conformal projection, and the Mercator projection. The governing equations of NHM are formulated for the arbitrary orthogonal curvilinear coordinate system on the sphere with the horizontal scaling factors of map projection, m_i defined by

$$ds_i = \frac{dx_i}{m_i} \quad \text{for} \quad i = 1, 2, \tag{1}$$

where ds_i is the length in the i-th direction when x_i varies with dx_i. Note that $m_1 = m_2$ in the conformal projections. If we take 1 and 2 in the longitudinal and latitudinal direction respectively, these map factors take the form;

$$(m_1, m_2) = \left(\frac{1}{a\cos\phi}, \frac{1}{a}\right) = \frac{1}{a}\left(\frac{1}{\cos\phi}, 1\right) \tag{2}$$

for the lat-lon coordinate, and

$$(m_1, m_2) = \left(\frac{\cos\phi_0}{\cos\phi}, 1\right) \tag{3}$$

for the CE projection, where a is the radius of the Earth, ϕ the latitude, and ϕ_0 the standard latitude. In case of $\phi_0 = 0$, the CE projection is equivalent to the lat-lon coordinate except for its coordinate dimension; it is length in the CE projection while angle in the lat-lon coordinate.

To test our implementation of the CE projection, three runs of 18 hours forecast were performed on a HITACHI SR8000 distributed memory parallel supercomputer. The configuration of test runs is summarized in Table 1. Figure 1 shows a result of two runs with same configuration except for their map projection. The CE projection (Fig. 1b) reproduced the reference result with the Lambert conformal projection (Fig. 1a). Another preliminary run for large domain is also performed using GANAL of JMA as the initial and

boundary conditions (Fig. 2). Surface pressure pattern is well simulated, and the difference of domain averaged surface pressure between simulation and GANAL is within 1 hPa in the simulation period (18 hours).

Although the implementation of the CE projection was completed, two steps still remain to run NHM as a global model; re-implementation of the periodic boundary condition, and treatment for the grid points near the poles. Furthermore, from the view-point of computational efficiency, some kind of numerical technique to avoid the pole problem should be implemented; filtering longitudinal high-frequency modes near the poles, or the semi-Lagrangian scheme, and so on.

Table 1: Configuration of the test runs.

Name of the run	LM	CE1	CE2
Projection type	Lambert conformal	Cylindrical equidistant	
Standard latitude(s)	30N, 60N	35.5N	0N
Standard longitude	140.0E	–	
Center of the domain	133E, 35.5N		140E, 0N
Grid number	$289 \times 231 \times 40$		$121 \times 121 \times 40$
Horizontal resolution	10 km at the standard lat.		1 deg.
Vertical resolution	$40 \sim 1180$ m (40 levels)		
Initial condition	Meso 4D-Var[a)]		GANAL
Boundary condition	RSM[b)] forecast		GANAL

a) 4 dimensional variational data assimilation system for MSM (10 km mesh)
b) Regional Spectral Model of JMA (20 km mesh)

(a) Run-LM

(b) Run-CE1

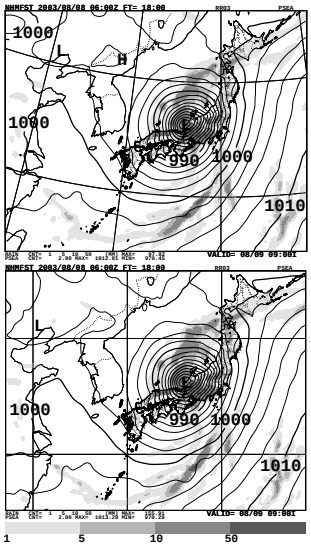

Figure 1: Sea-level pressure [hPa] (contour) and 3 hours precipitation [mm/3hours] (shaded contour) of 18 hours forecast; (a) Lambert conformal projection, and (b) CE projection. Initial time is 06UTC, 8 Aug., 2003.

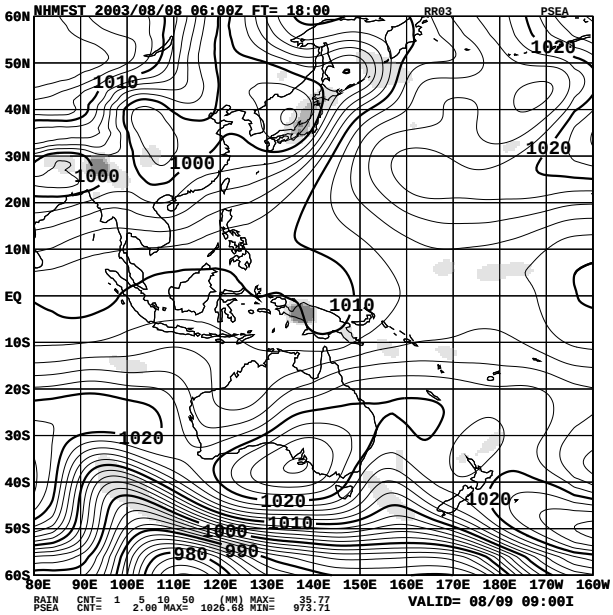

Figure 2: Same as in Fig. 1 but for large domain (Run-CE2).

References

[1] Saito, K., 2001: A global version of the Meteorological Research Institute/Numerical Prediction Division Nonhydrostatic Model, *CAS/JSC WGNE Research Activities in Atmospheric and Oceanic Modeling*, **31**, 6.20-6.21.

[2] Fujita, T., 2003: Higher order finite difference schemes for advection of NHM, *CAS/JSC WGNE Research Activities in Atmospheric and Oceanic Modeling*, **33**, 3.9-3.10.

[3] Saito, K., 2003: Time-splitting of advection in the JMA Nonhydrostatic Model, *CAS/JSC WGNE Research Activities in Atmospheric and Oceanic Modeling*, **33**, 3.15-3.16.